Simulations of light collection in long tapered CsI(Tl) scintillators using real crystal surface data and comparisons to measurement

Nuclear Inst. and Methods in Physics Research, A 1003 (2021) 165302

Contents lists available at ScienceDirect

Nuclear Inst. and Methods in Physics Research, A

journal homepage: www.elsevier.com/locate/nima

Simulations of light collection in long tapered CsI(Tl) scintillators using real crystal surface data and comparisons to measurement

A. Knyazev [a], J. Park [a,j], P. Golubev [a], J. Cederkäll [a,*], H. Alvarez-Pol [b], J. Benlliure [b], P. Cabanelas [b], E. Casarejos [c], L. Causeret [a], D. Cortina-Gil [b], P. Díaz Fernández [d], M. Feijoo [b], D. Galaviz [e], E. Galiana [e], R. Gernhäuser [f], D. Gonzalez [b], A.-L. Hartig [g], A. Heinz [d], B. Heiss [f], H.T. Johansson [d], P. Klenze [f], T. Kröll [g], A. Perea [h], L. Ponnath [f], Z. Ren [a], H.-B. Rhee [g], J.L. Rodriguez-Sanchez [b], G. Rondeau [a], O. Tengblad [h], I.G. Scheblykin [i], P. Teubig [e], R. Timm [a]

[a] Department of Physics, Lund University, SE-221 00 Lund, Sweden
[b] Dpt. de Física de Partículas, Universidade de Santiago de Compostela, E-15782 Santiago de Compostela, Spain
[c] Universidade de Vigo, E-36310 Vigo, Spain
[d] Department of Physics, Chalmers University of Technology, S-41296 Gothenburg, Sweden
[e] Laboratory for Instrumentation and Experimental Particle Physics, 1649-003 Lisbon, Portugal
[f] Physik Department, Technische Universität München, 85748 Garching, Germany
[g] Institut für Kernphysik, Technische Universität Darmstadt, D-64289 Darmstadt, Germany
[h] Instituto de Estructura de la Materia, CSIC, E-28006 Madrid, Spain
[i] Department of Chemistry, Lund University, SE-221 00 Lund, Sweden
[j] Center for Exotic Nuclear Studies, Institute for Basic Science (IBS), 34126 Daejeon, Republic of Korea

ARTICLE INFO

Keywords:
Calorimeters
Scintillators
Absorption length
Surface topography
Simulation of light transport

ABSTRACT

Simulation results for light transport in long tapered CsI(Tl) crystals using look-up tables (LUTs) are presented. The LUTs were derived from the topography of a polished and a lapped surface of a CsI(Tl) crystal measured with atomic force microscopy. Simulations with different combinations of polished and lapped surfaces were performed, to extract the non-uniformity of light collection depending on the interaction point, and compared to experimental results. The simulations reproduce the general trend given by the measurements, and show that more homogeneous light collection is attained when all lateral sides of the crystal are lapped. For the lapped crystal the simulation model is most sensitive to the reflectivity of the enhanced specular reflector (ESR) foil surrounding the crystal, which is one of several properties influencing the light transport examined in this study. The sensitivity of the light-output non-uniformity to variations in the absorption length observed in a batch of CsI(Tl) crystals in a previous study is also discussed. Residual differences between the simulation and the measurements can potentially be attributed to the scattering of scintillation photons inside the materials used. Additional measurements to further advance the construction of the simulation model are suggested.

1. Introduction

1.1. Purpose of the study

The purpose of this study is to investigate light transport in large-volume inorganic scintillators of CsI(Tl), used for nuclear calorimetry and spectroscopy, by exploiting a new promising simulation approach based on real crystal surface data that has become available recently [1,2]. A thorough understanding of light transport and collection in scintillation detectors for nuclear physics is of importance for the understanding of light-output uniformity, and consequently for the energy resolution that can be achieved with such detectors. We refer to Refs. [3,4] for a detailed background discussion.

A computer model that can describe this process with high accuracy would provide a valuable tool to predict the performance of a new detector system during the design phase, and can also be used in the manufacturing process. With the advent of improved crystal surface mapping techniques and increased computing power it is of interest to take advantage of these two developments for a comparison between simulated and measured data with a focus on improving light-output uniformity.

* Corresponding author.
E-mail address: joakim.cederkall@nuclear.lu.se (J. Cederkäll).

https://doi.org/10.1016/j.nima.2021.165302
Received 16 November 2020; Received in revised form 11 February 2021; Accepted 27 March 2021
Available online 1 April 2021

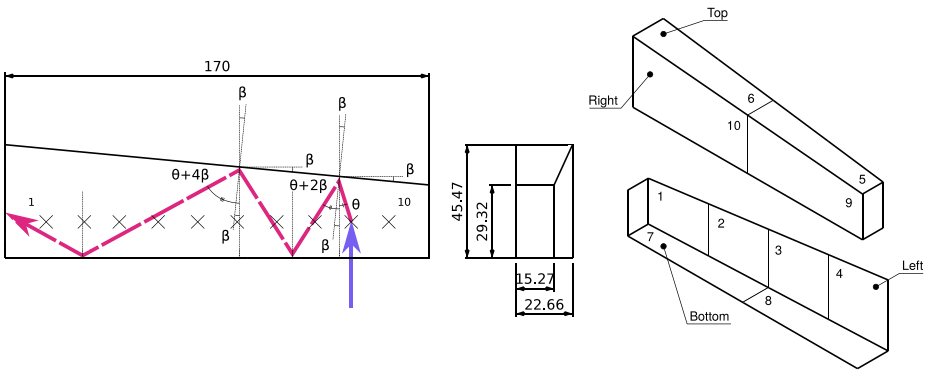

Fig. 1. To the left: a sketch of the CsI(Tl) crystal used for measurements and simulations of light transport in this work. The full blue arrow indicates an incident γ-ray. The measurements were performed with a collimated beam in 10 equidistant points indicated by crosses. The dashed red line illustrates the focussing effect caused by the tapered side of the crystal. The avalanche photo diode used for the light read-out is situated on the left side of the crystal. All distances are given in mm. To the right: the order followed when lapping the sides of the crystal. The lapping was applied to the indicated areas starting from area 1, and adding new surfaces, until area 10 was lapped. In the text this sequence is designated as lapping cases A to K. These cases corresponds to a fully polished crystal (A), and a gradual increase of the lapped area using the 10 indicated areas, until the crystal was fully lapped (K).

This work follows the development of the calorimeter, CALIFA [5], for the R^3B experiment [6] at FAIR [7]. CALIFA consists of commercially manufactured CsI(Tl) crystals[1] of elongated shape with lengths from 17 cm up to 22 cm, each of which is wrapped in enhanced specular reflector (ESR) foil[2] to aid optical photon transport and coupled to avalanche photodiodes (APDs)[3] for light readout.

1.2. Current status of light transport simulations for detectors in nuclear physics

Traditionally light transport models implemented in state-of-the-art simulation software, e.g. GEANT4 [8–10], have relied on parameter-dependent models where the relative influence of effects such as specular reflection, backscattering in groves on the surface, and diffuse Lambertian scattering are described by a set of parameters that can be challenging to determine empirically. Consequently, such models may introduce an amount of arbitrariness in the result if they include many parameters. An example of this parametric approach, which can be used for general discussions, is the well-established UNIFIED model [8–10], which contains 5 parameters that characterize the processes involved in the way indicated above.

However, recently it has also become possible to use look-up tables (LUTs) based on measurements that describe light scattering on the boundaries of a crystal. Two approaches that have provided promising results should be mentioned. The first one relies on the calculation of light reflection and transmission based on atomic force microscopy (AFM) measurements of the surface [1,2], while the second approach is based on direct measurements of the distribution of scattered light using a dedicated apparatus [11–13]. In this work we employ the first method and calculate LUTs based on surface maps from AFM measurements of lapped and polished surfaces, and apply them in simulations. The underlying principle of this method, to calculate a LUT for light scattering on the crystal boundary, is to extract the direction of the surface normal at each grid point based on the topographical map from the AFM measurement, to let photons scatter on this surface from all possible directions from inside the crystal, and to register the corresponding outgoing angles. In practice a random grid point on the surface is first selected and its normal is extracted. The wavelength of an incoming photon is then simulated based on the wavelength distribution of the scintillation spectrum of the material. Furthermore, the direction of the photon with respect to the boundary is also simulated by randomizing over all possible incoming directions. The resulting reflection angle, for a given incoming direction, is then calculated using mirror reflection and is stored in a two-dimensional histogram with the azimuthal and polar reflection angles on the two axes. The same procedure is also carried out for photons that transmit through the surface. In this case the transmission angle is calculated using Snell's law. The probability that reflection or transmission occurs is in turn given by the Fresnel equations. Further details of the calculation of the LUTs are given in Section 4.3. For completeness, we mention that the alternative method, that uses a dedicated apparatus, is based on the principle of shining a light beam through a half-sphere shaped crystal sample onto the boundary under investigation using a movable source, and to measure the corresponding spatial intensity distribution from the reflection using a likewise movable detector. For a more detailed discussion of the alternative method we refer the reader to Refs. [11–13].

The simulation results from the current investigation are compared to a set of light-output measurements for a large-volume crystal with the same geometry and surface treatments that are used in the simulations. A specific advantage with the AFM-based approach is that AFMs are commercially available and are in common use for surface characterization also in other scientific fields. One can also point out that by avoiding the parameter dependence inherent in earlier models one can now with more confidence investigate the dependence of the detector response on other important physical parameters, e.g. the absorption length and refractive indices of the materials involved. We also perform such a sensitivity study as part of this work.

2. Material-related simulation parameters

For light transport in tapered crystals, which are commonly used in detector systems with large solid angle coverage for high geometrical efficiency, two major effects need to be considered. The first one, light absorption, is governed by the mean free path of the scintillation photons in the material. The second is the focussing effect. This effect results from the tapered shape of the crystal, and is due to the decrease of the incoming angle, with respect to the exit surface normal, that the scintillation photons experience with the number of reflections they have undergone at the tapered side of the crystal (see Fig. 1). This effect can be reduced by surface treatment, which introduces a randomized distribution of microfacets on the surface that leads to a randomization of incoming angles for the scintillation photons on the exit surface. Both these effects have been discussed previously in the literature. For a more detailed discussion, including the influence of surface treatment, we refer to our previous paper [4] and references therein.

The interplay of the processes mentioned above defines the amount of light that propagates to the light sensor. Consequently, although

[1] Amcrys-h Ltd., Kharkov, Ukraine.
[2] 3M Company, Vikuiti 3000.
[3] Hamamatsu Photonics K. K., Si APD S8664-1010.

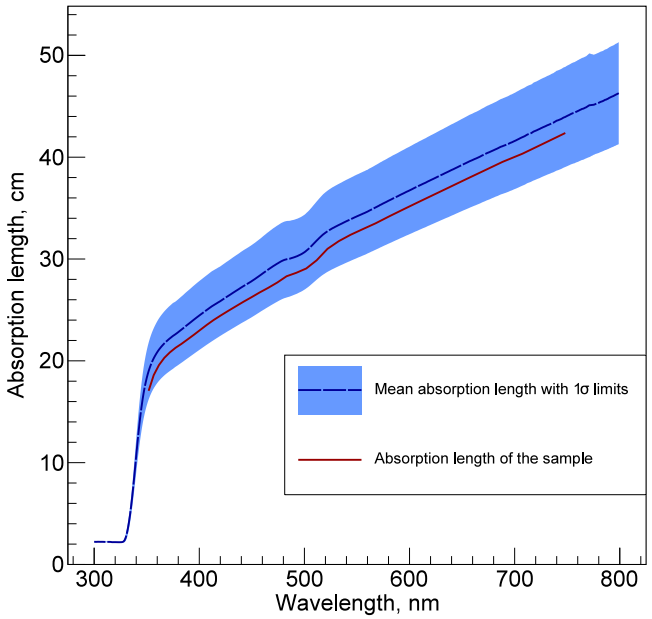

Fig. 2. The light absorption length in CsI(Tl), as a function of the photon wavelength, measured with a spectrophotometer. The dashed dark blue line shows the average absorption length for a sample of 10 crystals. The blue region indicates the 1σ band for the mean trend. The absorption length of the crystal used for the measurements and simulations of the light-output non-uniformity in this work is shown by the full red line.

Table 1
Nominal values of parameters used for the simulation of light transport in the tapered CsI(Tl) crystal in this work. The refractive index of CsI(Tl) is given as the weighted average over the scintillation emission peak, as is the reflectivity of the ESR foil and the two absorption lengths. The refractive indices of the window and the coupler is as provided by the respective manufacturer. For further information about the emission spectrum and the quantum efficiency of the APD, which were kept constant in this work, we refer to our previous publication [4] that discusses the light readout from the experimental point of view. For further information about the absorption lengths see Fig. 2 and the corresponding information given in the text.

Simulation parameter	Notation	Nominal value	Unit
Refractive index of window	n_w	1.53	
Refractive index of optical coupler	n_c	1.41	
Refractive index of CsI(Tl)	n_{CsI}	1.80	
Reflectivity of ESR foil	R_{ESR}	99.52	%
Mean absorption length	λ_{mean}	32.83	cm
Crystal absorption length	λ	31.15	cm

the introduction of LUTs, based on realistic surfaces, removes several parameters from the light transport simulation, a number of material-dependent parameters still need to be taken into account. In addition to the absorption length these include the reflectivity of the reflector foil, the refractive indices of the crystal, the optical coupling material, and of the window of the photo sensor itself. The refractive indices are important since they determine how much of the light reflects or traverses the crystal boundaries. For the simulations described below the refractive index of the crystal was estimated with a set of parameters from Ref. [14], while the refractive indices of the coupler and the window were obtained from the data sheets of the respective manufacturers. The influence of these two parameters on the uniformity of the light collection is discussed further in Section 5.2. Another physical property to consider is the emission spectrum of CsI(Tl), which is known to be dependent on the dopant concentration [15]. In this work the emission spectrum given in Ref. [16] was used. A summary of the nominal values of the parameters that were used in the simulation is given in Table 1 with additional description below.

2.1. Measurement of the absorption length

A 17-cm CsI(Tl) test crystal of the shape shown in Fig. 1 was used for these measurements. A spectrophotometer[4] was employed to obtain the absorption length measured along the main axis of the test crystal. The measurement procedure to extract the absorption length is described in more detail in Ref. [4]. The apparatus uses a sample beam of variable wavelength and measures the attenuation of the light intensity as the beam traverses the material and is detected on the receiving end. In this work a wavelength range from 300 nm to 750 nm was used to cover the emission spectrum of CsI(Tl). The attenuation was extracted taking into account the refractive index of CsI and the reflection on the entrance and exit surfaces assuming a single passage of the light beam. This assumption should be precise to $\lesssim$1% (see Ref. [4] for further discussion).

A first set of measurements, to establish the mean value for the attentuation length and the standard deviation for the crystal material, were performed on a set of 10 crystals (see Fig. 2) as described earlier [4]. The measurement of the absorption length of the test crystal investigated here was performed in the same manner. Its attenuation length (see Fig. 2, red curve) was found to be smaller than the average value from previous measurement, but well within the 1σ deviation. In the wavelength range from 500 nm to 600 nm, where the CsI(Tl) emission spectrum is the most intense, the attenuation length increases from 28 cm up to 34 cm for the test crystal. Supplementary measurements with and without ESR foils surrounding the four long sides of the test crystal were performed in order to gauge the amount of beam scattered out of the crystal volume. No significant differences ($< 2\%$) were found between these two measurements.

2.2. Measurement of the surface topography

A test sample in the form of a $1 \times 1 \times 1$ cm^3 cube of CsI(Tl) was used for the surface measurements. The size of the test sample was determined by the maximum sample size that could be well fitted into the atomic force microscope. The sample was obtained from the manufacturer of the CsI(Tl) crystals used for the CALIFA project. The treatment of the surfaces was performed using the same procedure that was applied for the 17-cm test crystal as discussed in Section 3. The polishing was performed with ethylene glycol and a polishing tissue and lapping was performed with a P1200 abrasive. The surface topographies of the two surface types were measured with an AFM[5] on 100×100 μm^2 test areas. The procedure is described in more detail in Ref. [4]. The results are presented in Fig. 3. Typical quantities used to characterize the roughness of a surface [3] include the root-mean-square (RMS) σ_z, of the surface height, z, defined as:

$$\bar{z} = \frac{1}{N}\sum_{i=1}^{N} z_i, \tag{1}$$

$$\sigma_z = \sqrt{\frac{1}{N}\sum_{i=1}^{N}(z_i - \bar{z})^2}, \tag{2}$$

where N is the number of gridpoints, z_i designates the height over a fitted reference plane in the i:th gridpoint, and $\bar{z}$ is the mean height. Furthermore, it is also common to extract the slope pointwise over the surface using adjacent points. The slope in point, k, is defined as:

$$m_k = \frac{z_{k+1} - z_k}{\tau_0}, \tag{3}$$

where distance between the grid points, $\tau_0 = 100$ nm in this study. The corresponding average of the slope, m, and its RMS were calculated using the same general definitions that were used for the mean of the height and its RMS. The difference in the RMS of the surface height

[4] PerkinElmer, LAMBDA 1050UV/Vis.
[5] Bruker GmbH, JPK Nanowizard II.

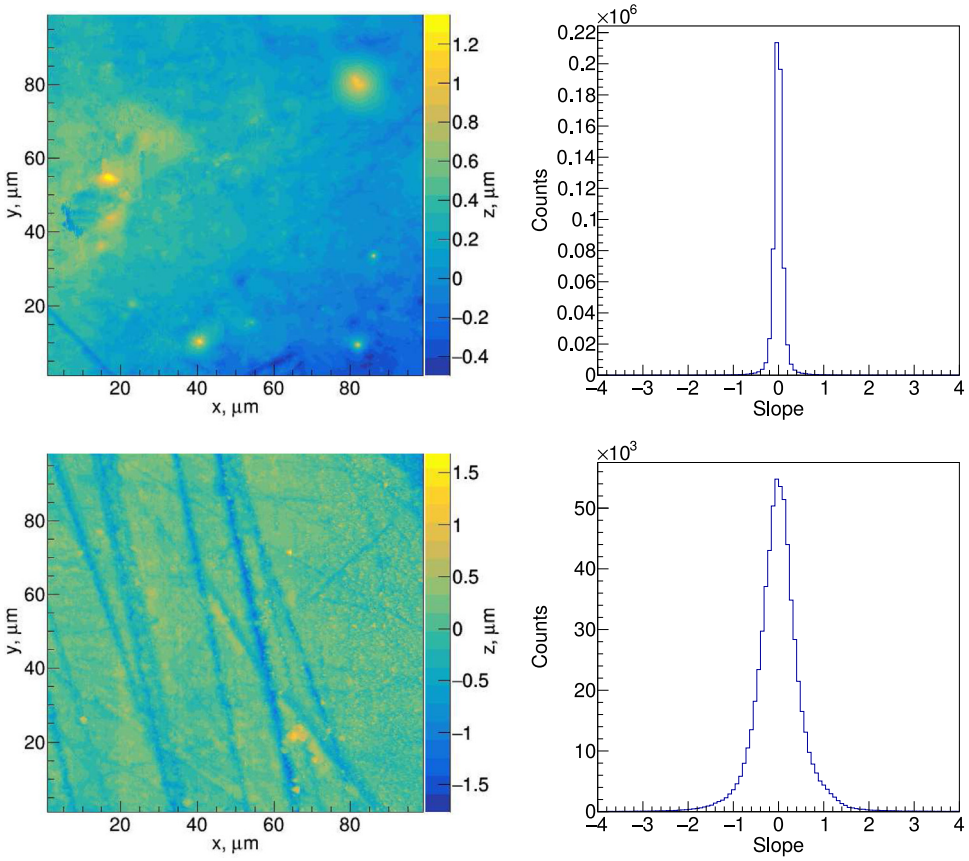

Fig. 3. Results of the surface topography measurements. The top row shows results for the polished, and the bottom row for the lapped surface, with the surface maps and slope distributions in the left and right columns, respectively.

of the polished and lapped areas was rather small and was found to be 0.22 µm for the polished and 0.23 µm for the lapped surface. The difference between the two surfaces are more pronounced in the RMS of the slope distribution, σ_m, which was found to be 0.15 for the polished and 0.54 for the lapped surface, respectively.

3. Measurement of light-output non-uniformity

3.1. Preparation of the test crystal

For this series of measurements, the same test crystal was used as in the spectrophotometer measurements of the absorption length. In order to investigate the dependence of the uniformity of light collection on the surface treatment, and to see to what extent state-of-the-art simulations can reproduce the measurement results, it is of interest to provide a set of measurements for varying amounts of lapping applied to the crystal surface. To achieve this the total lapped area on the test crystal was increased gradually and the response of the crystal was measured along the crystal main axis.

Specifically, the surface of the crystal was divided into 10 sectors (see the right side of Fig. 1) and each sector was successively treated until all lateral sides of the crystal were lapped. These surface treatment cases are labeled from A to K below, where A corresponds to the fully polished case, B means that sector 1 is lapped, C that sectors 1 and 2 are lapped etc until all lateral sides are lapped, which is denoted as case K.

3.2. Measurement procedure

The light output non-uniformity as a function of source position was quantified using ΔLO, defined as:

$$\Delta\mathrm{LO} = \frac{x^{(c)}_{\max} - x^{(c)}_{\min}}{\frac{1}{N}\sum_{i=1}^{N} x^{(c)}_i}, \tag{4}$$

where $x^{(c)}_i$ is the photo peak centroid and N is the number of irradiation points along the main axis. For the measurements discussed here ΔLO of the sample was extracted from 10 equidistant points with an intervening distance of 15.5 mm. A collimated ^{137}Cs γ-ray source was used for production of the scintillation light. The emittance of the beam of 10 msr resulted in a beam spot of ~15 mm diameter on the entrance surface of the crystal. The scintillation light was detected by a large area APD as described above. We have in previous work performed an investigation of the APD, specifically concerning its temperature sensitivity and the effectiveness of temperature stabilization using the dependence of the gain on the bias voltage. For further information about measurement setup and the APD we refer to Ref. [4] where information about the quantum efficiency and the responsivity as a function of wavelength is given as well.

The non-uniformity of the light output was extracted for each lapping treatment. The result is shown in Fig. 4. The general trend is that ΔLO decreases with increased lapped area and that lapping of the large lateral sides (left or right as indicated in Fig. 1) is most important. Note, however, for example that by lapping three quarters of the left side according to lapping case D, the ΔLO is reduced from 12.4% to 6.8%, i.e. almost by 50% with respect to lapping only the furthest most half of the left side (case C). Consequently, the relation between the

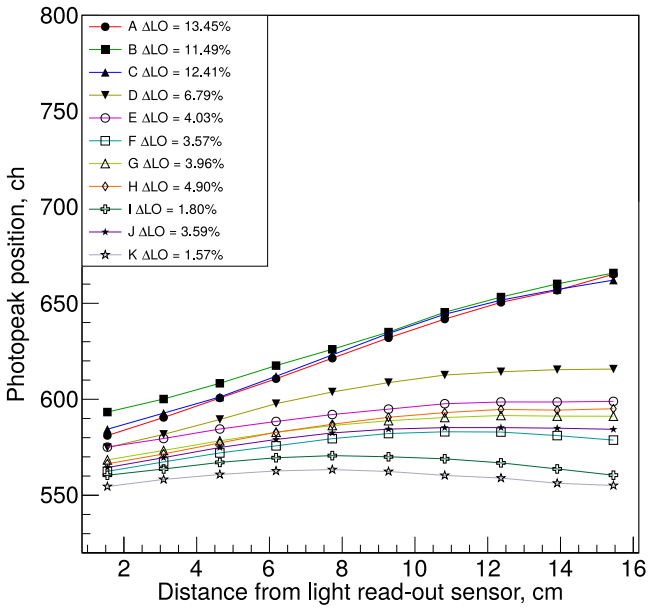

Fig. 4. Results of the light output non-uniformity measurements obtained with a collimated ^{137}Cs source. The peak position as a function of distance to the light sensor is shown for different lapping cases (see Fig. 1). The maximum relative differences for each case, ΔLO, (see text) is shown in the inset.

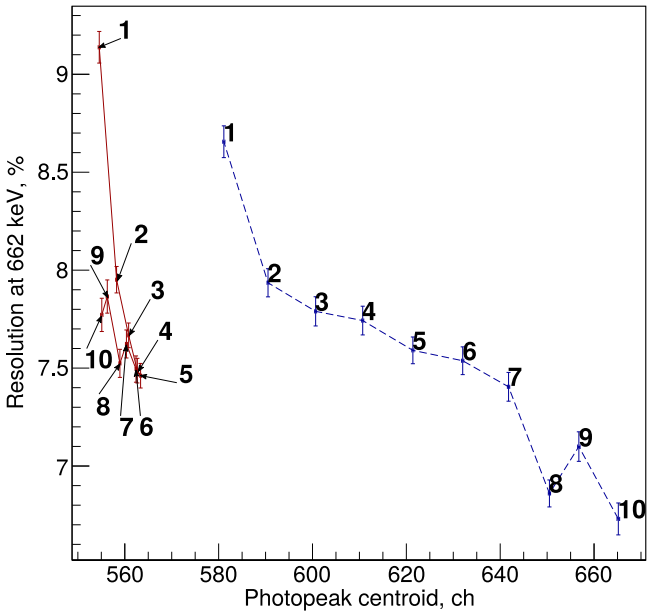

Fig. 5. The relation between the energy resolution of and centroid for a photopeak registered by the 17 cm long CsI(Tl) crystal, irradiated by a collimated ^{137}Cs γ-ray source in 10 equidistant points (see Fig. 1) along the main crystal axis. The irradiation points are indicated by numbers, with point 1 being closest to the photo sensor and point 10 furthest away. The dashed blue line shows the trend for the completely polished crystal, and the red line for the crystal with all lateral sides lapped (case K in the text). The lapping compresses the trend curve and thus reduces the influence of the light collection on ΔLO.

lapped area and ΔLO is non-trivial and is not defined by an inversely proportional relationship.

The dependence of ΔLO on the surface treatment can also be illustrated by the correlation between the ^{137}Cs photo peak centroid and its resolution for the fully polished and fully lapped crystal (see Fig. 5). One can see the lapped crystal exhibits only small variations in the centroid positions and thus possesses an improved energy resolution in a realistic scenario where the position of the scintillation vertex inside the crystal volume is arbitrary. One exception is the point closest to the photo sensor, which deviates significantly from the general trend that can be seen for the other points. This indicates that the measurement in this point may be influenced by edge effects due to scattering of large parts of the scintillation light on the readout surface. A similar qualitative behavior was also observed for the point closest to the readout sensor in the simulation. This is discussed further in Section 5.

It should be mentioned that the reproduction of the actual resolution was not the goal of the simulations as this would involve additional uncertain parameters. One would in that case e.g. have to introduce the Fano factor into the model which is outside of the scope of the current study.

4. Simulations

4.1. General description of the simulations

As mentioned above, in this work the GEANT4 [8–10] framework (version GEANT4.10.05.p01) was used to simulate the uniformity of the light collection from different parts of the crystal volume. In addition to the recent development to include light reflection and transmission for surfaces with realistic topography, GEANT4 allows to use material-specific properties in the simulation. In this case, the scintillator response was described by the emission spectrum of the optical photons in CsI(Tl) [16], and by its wavelength-dependent refractive index and absorption length. The refractive index was calculated using the parameters from Ref. [14], as indicated above, and the absorption length was extracted from the measurements described in Section 2.1. The nominal values for these material parameters are summarized in Table 1 as mentioned above. It should be mentioned that the material

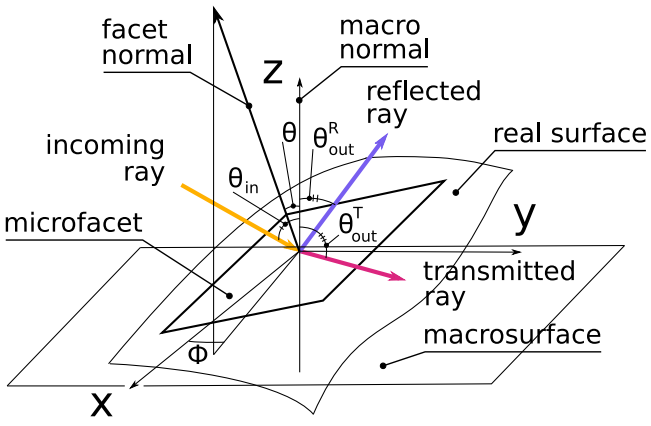

Fig. 6. An illustration of the microscopic approach to the simulation of real surfaces. The surface is considered as a set of microfacets oriented with respect to the normal of the macro surface. The θ and φ angles give the orientation of the microfacet normal with respect to the macrosurface normal. θ_{in} indicates the incident angle, θ^R_{out} and θ^T_{out} show the angles of reflection and transmission with respect to the macrosurface normal.

properties can be added in GEANT4 following standard procedure, using dedicated calls in the detector construction routine. The approach is well described in the GEANT4 documentation and we thus refer the reader to Refs. [8–10] for further information and additional references detailing how this functionality is included in GEANT4.

The simulation of the interaction of the 662 keV γ-ray beam, used in the measurements, with the CsI(Tl) material, was implemented using the Livermore model [17,18] for the photoelectric effect and for Rayleigh scattering, while the Monash model [18] was used for Compton scattering. The processes of ionization, bremsstrahlung and multiple scattering were activated to simulate the trajectories of the electrons that are knocked-out from the atoms during γ-ray detection.

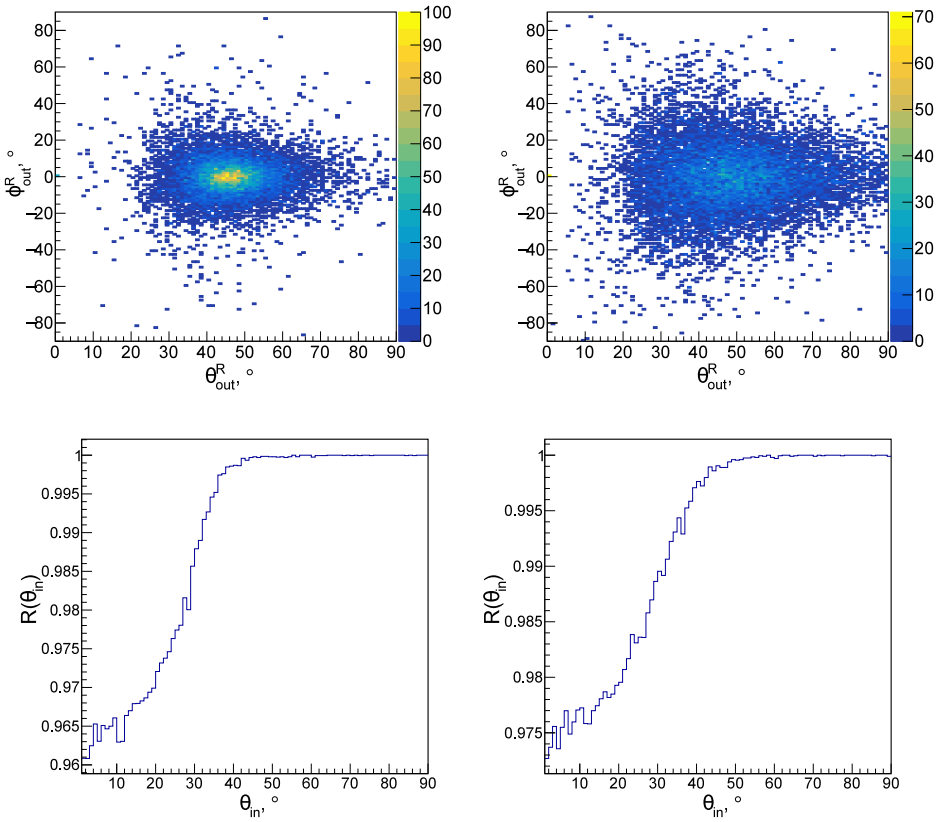

Fig. 7. Look-up tables and reflectivity curves for the simulations. Top left: distribution of the angles of reflection for the incident photon at $\theta_{in} = 45°$ and $\varphi_{in} = 0°$ for the polished surface. Top right: the same for the lapped surface. Bottom row: reflectivity curves for the polished and the lapped surfaces respectively. Note that white pixels contain zero counts. For definition of the angles see Fig. 6 and for further discussion see the text.

For the optical photons, bulk absorption was used as an approximation. The absorption was also investigated in separate simulation runs, using the geometry of the spectrophotometer measurement, in order to verify that the simulation reproduced the expected result, before more complex surface treatments were introduced. A potential expansion of the simulation would be to investigate the effects of Mie and Rayleigh scattering in detail. One can note however, that the implementation of Mie scattering in GEANT4 relies on four different parameters that potentially can be fitted. However, in these first simulations using real surface data we aim to introduce a minimum of free parameters and prefer to revisit those processes in future work. In general terms scattering of the scintillation photons on imperfections in the crystal will lead to deflection of the photons in their path and be experienced as crystal dimming. Such scattering would consequently mean that part of the photons will not propagate according to the path predicted by the simulation but could deviate towards the side surfaces where they can reflect towards the readout sensor along a new path or leave the crystal altogether. This effect could therefore also influence light collection from different parts of the crystal depending on where the crystal imperfections are located, and how significant they are. For a discussion of the effects that Mie scattering can have on photon propagation and collection, we refer to e.g. Ref. [19].

4.2. Description of the model

The geometrical model of the 17-cm long crystal shown in Fig. 1 was used to describe the scintillator, and a double APD (two 10 × 10 mm^2 segments) was implemented as detector for the optical photons. The geometry of the simulated detection surface and materials matched the physical geometry of the APD. The quantum efficiency of the APD as a function of the photon wavelength was extracted from the manufacturer catalogue [20].

The simulation mimicked the measurement procedure such that the scintillator was irradiated in the 10 equidistant points along the main axis. The position and the emittance of the γ-ray beam were taken from the measurement set-up described in Section 3.2. The processes of transmission and reflection of optical photons were simulated using the framework implemented in GEANT4 for the optical surface model developed at University of California Davis (UC Davis) [1]. For the simulations we first measured the surface topographies, for the CsI(Tl) material and surface treatments as described above, in order to calculate new LUTs for our case of interest. The calculation of the LUTs is discussed in the following section where we refer to this model for surface reflection LUTs as the Davis model, following the naming convention in the GEANT4 documentation.

4.3. Calculation of LUTs

In the Davis model [1], the scattering of optical photons on the boundaries of the medium is described by a θ-φ distribution for a set of incoming angles. A reflectivity curve is also calculated for the set of incoming angles.

For this study we wrote a program to calculate the θ-φ distribution from the surface topography using a Monte Carlo approach. A random point is selected on the surface. This defines the direction of the microfacet (see Fig. 6). The outgoing direction of a scattered optical photon is determined from the Fresnel equations for each incoming angle to decide if it should be reflected or transmitted. The transmission angle is calculated using Snell's law, while specular reflection with respect to the microfacet normal is assumed for reflection back into the crystal. The program also ensures that the scintillation photons created in the simulation hit the boundary from the inside of the crystal volume.

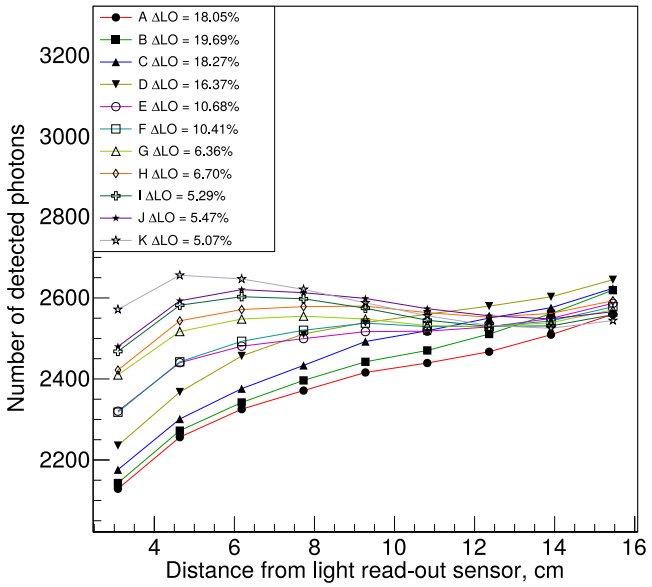

Fig. 8. Results from the simulation of the light-output non-uniformity for the 17 cm long CsI(Tl) crystal used in this work. See the text for the lapping strategy scheme. The simulations reproduce the general trend for ΔLO from the measurements, yielding the lowest light-output non-uniformity for the fully lapped case (case K). See also Fig. 4.

The angles of reflection and transmission constitute the θ-φ distributions and the ratio of transmitted/reflected light is stored in the reflectivity curve. An additional θ-φ distribution LUT, together with the reflectivity curve, is calculated for the light scattering from the outside into the scintillation material.

These two LUTs were in this work then used in combination to describe scattering from the crystal to the reflector and back into the crystal. When the light is transmitted out of the crystal, the reflection angle in the reflector is calculated assuming specular reflection, with a reflection probability defined by the reflectivity of the reflector foil. The entrance point of the photons, which are transmitted back into the crystal, is assumed to be in the same as position where the initial scattering happens. This is a simplification made to save computation time but is also necessary when using the Davis model for a combined interface, including a detector medium and a reflection foil. When the reflected light scatters on the surface of the crystal, the outgoing angles are again defined by the LUT, but now for scattering from the outside into the detector material.

The light may also scatter out of the detector completely. In that case it scatters on the reflector and crystal until it transmits into the outer volume, or the number of reflections exceeds a preset limit for the number of reflections. With this approach, a reflection and transmission angle, and a corresponding reflectivity curve, can be calculated for each incoming direction producing a combined LUT. Such LUTs, for the polished and lapped surfaces, respectively, were used in the simulations of the light collection discussed here to account for the different surface treatments (see Fig. 7). The framework described above has the advantage that it can account for the properties of the reflective material, commonly used together with scintillators to prevent leakage of photons, while still allowing photon leakage out from the medium, i.e. photon transmission.

5. Result and discussion

5.1. Measurements and simulation results for nominal parameters

As can be seen from the measurements presented in Fig. 5, the photo peak measured for the source position closest to the photo sensor has the smallest amplitude, i.e. centroid position, of the 10 irradiation points, and also the lowest resolution for the polished crystal. When lapping is applied on all the lateral sides the centroid positions of the photo peaks group more closely together and also exhibit a slightly lower energy resolution. This applies as well to the irradiation point closest to the sensor, i.e. it moves to approximately the same centroid position as the other photo peaks, but having already an outlier position when it comes to resolution it cannot be brought closer to the main cluster formed by the other nine irradiation points on the resolution axis of Fig. 5. To some extent this behavior was also reproduced in the simulations. The point closest to the photo sensor had the lowest photo peak amplitude and the lowest resolution, to the level that with the runtime-limited statistics obtained, it was non-trivial to obtain a good fit for that point for all simulated lapping cases and to facilitate a reasonable comparison between simulations and measurement for the full set of cases. For this reason we have excluded this point for the comparisons of light output uniformity below. This can also be motivated by the fact that the centroid and resolution for the irradiation point closest to the sensor will depend more on the amount of scintillation photons that traverse directly towards the readout surface than for points that are further away. One can mention two main features in this context. On the one hand the point closest to the sensor sees the exit window under a larger solid angle than the other points, and photons that propagate in the direction of the sensor might therefore experience relatively fewer reflections on the boundaries, making the focussing effect less pronounced for this point. On the other hand those photons that propagate in the opposite direction to the sensor would in a simplified picture have to travel two times the crystal length to arrive at the exit window, and would therefore experience more attenuation. One can also note that this irradiation point leads to a γ-ray path through the crystal where scintillation photons, arising from a photo effect event, which propagate directly towards the readout sensor, will have largely varying angles with respect to the normal of the exit surface. This means that depending on where the scintillation photons are created along the path of the γ ray they will transmit through the boundary and be registered by the APD with varying probability. As an effect, scintillation events that occur towards the top or the bottom surfaces (see Fig. 1) will see a different amount of photons being detected compared to events that occur e.g. halfway into the crystal. The result is a broadened and thus less distinct photo peak. This effect is similar to the focussing effect for a polished crystal with the difference that it is not influenced by the lapping of the side surfaces, which is the topic of the current study.

Consequently, from the preliminary investigation of the first irradiation point we have concluded that it requires a dedicated set of measurements to benchmark simulations for this point. However, in order to determine at which distance this effect becomes important it is needed to carry out detailed measurements close to the sensor using a highly collimated, and thus stronger, source than was available for the current study.

Table 2
Comparison of measurement and simulation results for different lapping cases. The difference between the second and third column is the removal of the first data point in the ΔLO determination. For discussion see text.

Case	ΔLO_{sim}, %	$\Delta LO_{exp}^{N=9}$, %	ΔLO_{exp}, %
A	18.0	13.3	13.4
B	19.7	11.4	11.5
C	18.3	12.3	12.4
D	16.4	6.8	6.8
E	10.7	4.0	4.0
F	10.4	3.6	3.6
G	6.4	4.0	4.0
H	6.7	4.9	4.9
I	5.4	1.8	1.8
J	5.5	3.6	3.6
K	5.1	1.6	1.6

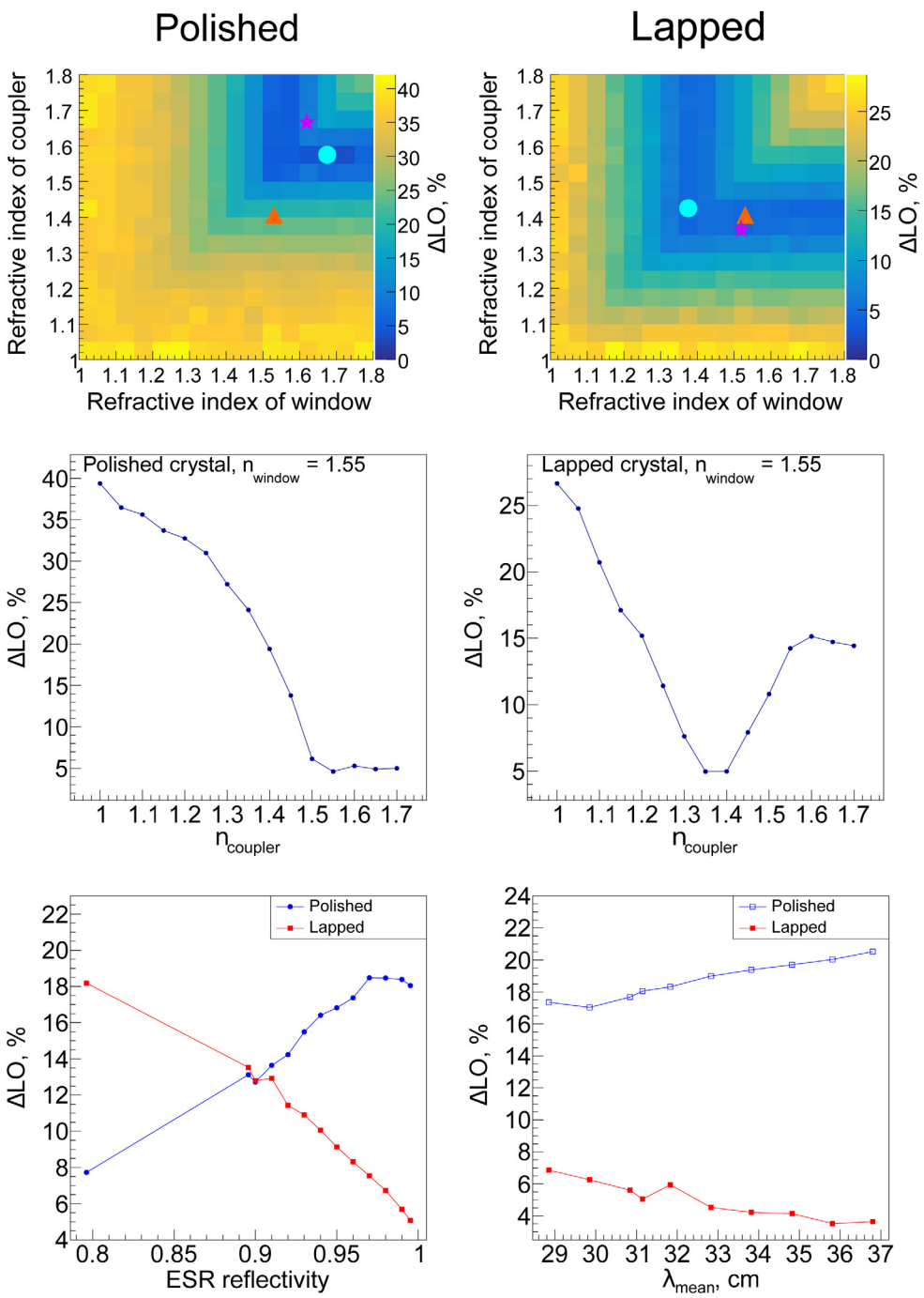

Fig. 9. Results of the sensitivity tests for different parameters used in the simulations. Top row: sensitivity of light-output non-uniformity as function of the refractive indices of the coupler and the window for the polished and the lapped crystal, respectively. The filled triangle indicates the nominal factory values for the respective indices of refraction. The filled circle shows which combination of the two refractive indices that would lead to the minimum light-output non-uniformity according to the simulation. The filled star gives the two indices of refraction that correspond to the minimum chi-square between the measurement and simulation over the nine simulated points. Center row: Light-output non-uniformity for the refractive index of the window, $n_w = 1.55$, for the polished (left) and fully lapped (right) crystal. Bottom left: sensitivity of ΔLO with respect to the ESR reflectivity used for the calculation of the look-up tables for the polished and lapped surface. Bottom right: the dependence of ΔLO on the absorption length of the crystal. If not otherwise stated, the non-varying parameters were kept at their nominal values. For clarity we expand the abbreviations w for window and c for coupler used in Table 1 for these graphs.

The results of the simulations are presented in Fig. 8 and the ΔLO from the measurements and the simulations are given in Table 2. One can note that for the measurements there is only a small difference in ΔLO_{exp} extracted for ten and nine irradiation points, where the latter are used for the comparison with the simulations.

The general trend for ΔLO as a function of the lapped area is largely reproduced by the simulations. A decrease from a non-uniformity of 13.5% to 1.6% is observed experimentally, while the simulations predict an improvement from 18.0% to 5.1% from a fully polished to a fully lapped crystal. An important difference between the measurements and simulations is the total light output detected by the photo sensor. During the measurement, the total light output decreased with increased total lapped area (see Fig. 4) while the results of the simulations show the opposite behavior. Lapping increases the total light

output, although making the differences between the irradiation points smaller. This effect can potentially be attributed to the fact that in these simulations we aimed to minimize the number of unknown parameters and therefore made no attempt to fit any Mie scattering parameters to the global data since such an approach would introduce an additional level of arbitrariness. Additional scattering in the crystal may explain the increased absorption, or loss of photons, observed in the measurements of the lapped crystal, but other effects could do so as well. One can e.g. measure the reflectivity of the foil as a function of the incoming angle of a photon, and also perform actual measurements of the refractive indices of the optical coupler and the window of the APD instead of using the manufacturer data. If e.g. the reflectivity of the foil would have a strong angular dependence one can speculate that more light could escape the detector module after lapping.

As discussed above it is also interesting to note that there are certain lapping cases between which ΔLO decreases rapidly. This feature is observed also in the simulations, but it should be pointed out that they do not correspond to the same cases as in the measurements. For the simulation an improvement from 16.4% to 10.7% is observed when going from the left surface being 75% to 100% lapped, while a corresponding drop from 12.3% to 6.8% is observed in the measurement going from 50% to 75% lapping of the same surface. Furthermore, a second drop in non-uniformity, from 10.4% to 6.4% is observed in the simulation between cases F and G, where the left side is fully lapped and the top surface goes from 50% to 100% lapping. In the measurement a second drop in non-uniformity is also observed. In that case it happens between cases H and I, corresponding to the left and top sides being 100% lapped and the bottom surface going from 50% to 100% lapping.

5.2. Sensitivity tests

Since the general trend of ΔLO with respect to the applied lapping is reproduced in the simulations, but with some discrepancies still remaining i.e. concerning the smallest achievable non-uniformity and the total light output, it is of interest to investigate the sensitivity of the results with respect to the physical input parameters, and thus the precision to which they are known. Knowledge of the sensitivity to the specific input parameters is ultimately also of interest in order to guide the manufacturing process as a successful simulation model should be able to tell within which limits a certain parameter, e.g. the absorption length, should fall in order to obtain a non-uniformity within given specifications. The simulation model should also, based on a result for the non-uniformity, be able to predict the resolution that can be achieved when the physical parameters have a given statistical spread after manufacturing. Using the simulation model, we have performed sensitivity tests of this kind for four parameters, the refractive indices of the coupler and the sensor window, the light absorption length, and the reflectivity of the ESR foil used for calculation of the LUTs.

The results of these simulations for the fully polished and fully lapped crystal are presented in Fig. 9 where the two-dimensional histograms in the top row show the light-output non-uniformity, ΔLO, for different indices of refraction of the coupler and sensor window. The nominal values for these two parameters, 1.53 for the sensor window and 1.41 for the coupler, are indicated by the triangles in the two histograms. For these simulations the reflectivity of the ESR foil was set to 99.52% (see Ref. [4]) while the absorption length was given by the measured (red) curve in Fig. 2. The minimum ΔLO obtained in the respective scans is indicated by the filled circle in the histograms. For the fully lapped case the scan gives a minimum ΔLO of 4.14% for a refractive index of 1.35 for the sensor window and 1.4 for the coupler, to be compared to the 5.07% for the nominal parameter set and 1.57% for the measurement. A profile through the two 2D surfaces at a constant refractive index for the coupler, n_{window}=1.55 is given in the central row of Fig. 9. The respective gradients, defined as the rate of change of ΔLO with respect to the given parameter, were extracted to be −0.56 and 8.7 for the window and coupler refractive indices, respectively, meaning e.g. that for an increase of the refractive index of the coupler by 1% the ΔLO increased by 8.7% relative to the nominal value.

The light output curves, calculated from scanning the refractive indices in the simulations, were also compared to the measured ones using the chi-square between the two. In this context the chi-square is defined as the sum of the squared differences between the simulated and measured light-output curves in the nine irradiation points. The refractive indices giving a minimum chi-square are indicated by the filled stars in the two-dimensional histogram. For the lapped crystal the minimum chi-square occurs close to the nominal values, and the difference in the light-output non-uniformity, ΔLO, is only 0.93% between these points. These results indicate that the precision with which the refractive indices are known here does likely not cause the difference in observed and simulated ΔLO of 1.7% and 5.1%, respectively.

Furthermore, the analysis of the simulations for the lapped crystal shows that close to the nominal parameters, the ΔLO is most sensitive to the reflectivity of the ESR foil, where an increase of the reflectivity by 1% of the nominal value results in a relative change of the light-output non-uniformity by −18.9% with respect to the value obtained for the nominal reflectivity. In practice this means that an increase of the reflectivity of the foil from 99.52% to 100% would improve the non-uniformity from 5.1% to 4.6% (see bottom row in Fig. 9).

The corresponding dependence of ΔLO on the light absorption length is less sensitive. It changes by 2.1% when the absorption length is increased by 1% from the nominal value. For the absorption length one can therefore conclude that if two crystals exhibit a difference of $\pm 1\sigma$ in absorption length, as shown by the blue region in Fig. 2, they would according to the simulation (lower right panel of Fig. 9) have a light-output non-uniformity of 6.9% and 3.6%, respectively.

6. Summary and conclusion

The introduction of the Davis model [1] in light collection simulations, using look-up tables to describe optical surfaces based on real surface data, allows to circumvent the arbitrariness that alternative parameter-based models might introduce. With this it also becomes possible to investigate the effects of other physical parameters that are needed in the simulations, and which can be extracted from measurements, with more confidence. In this work light collection simulations were performed using the absorption length obtained from a spectrophotometer measurement and LUTs calculated from real surface topography measured with an AFM. Previously established refractive indices for CsI [14], as well as for the photo sensor window, and the corresponding light coupler were introduced and their influence on the simulation results was investigated. The simulations were compared to a set of measurements of the light-output non-uniformity, ΔLO, of a sample crystal. The simulations reproduced the general trend for ΔLO as extracted from the measurements. An important difference between the measurements and the simulation results is, however, that although lapping improves the light-output uniformity in both cases, the total light output is higher after lapping in the simulation but lower in the measurements. The trend of the light-output curve is consequently different. In the simulation the irradiation points closest to the photo sensor exhibit enhanced light output after lapping, leading to a reduced non-uniformity, while the measurement shows decreased light output, with an emphasis on the irradiation points furthest away from the sensor.

Finally, since the simulation shows similar improvement in light-output uniformity with increased lapping area as the measurements, but the measurements show an overall light loss with increased lapping area, it is suggested that lapping leads to an additional light loss mechanism that is currently not included in the simulations. Additional absorption effects such as Mie scattering can be included in the simulations in the future to establish potential contributions from this effect.

Other effects that may also give rise to additional light loss can be e.g. angular dependence of the reflectivity and transmission of the ESR foil. Both these effects are planned to be investigated in future work in order to improve the predictive power of the simulations.

CRediT authorship contribution statement

A. Knyazev: Methodology, Software, Validation, Formal analysis, Investigation, Data curation, Writing - original draft, Writing - review & editing, Visualization. **J. Park:** Methodology, Software, Formal analysis, Investigation, Writing - review & editing, Visualization. **P. Golubev:** Methodology, Software, Investigation, Writing - review & editing. **J. Cederkäll:** Conceptualization, Methodology, Software, Validation, Formal analysis, Investigation, Resources, Data curation, Writing - original draft, Writing - review & editing, Visualization, Supervision, Project administration. **H. Alvarez-Pol:** Conceptualization, Methodology, Software, Writing - review & editing, Supervision. **J. Benlliure:** Conceptualization, Methodology, Resources, Supervision. **P. Cabanelas:** Methodology, Writing - review & editing, Supervision. **E. Casarejos:** Conceptualization, Methodology. **L. Causeret:** Methodology, Software. **D. Cortina-Gil:** Conceptualization, Methodology, Resources, Supervision, Project administration. **P. Díaz Fernández:** Methodology. **M. Feijoo:** Software. **D. Galaviz:** Methodology. **E. Galiana:** Methodology, Validation. **R. Gernhäuser:** Conceptualization, Methodology, Software, Resources, Writing - review & editing, Project administration. **D. Gonzalez:** Validation. **A.-L. Hartig:** Validation. **A. Heinz:** Methodology, Writing - review & editing, Supervision. **B. Heiss:** Software. **H.T. Johansson:** Methodology, Software. **P. Klenze:** Software. **T. Kröll:** Resources, Supervision, Project administration. **A. Perea:** Software. **L. Ponnath:** Software. **Z. Ren:** Investigation. **H.-B. Rhee:** Validation. **J.L. Rodriguez-Sanchez:** Software. **G. Rondeau:** Software, Writing - review & editing. **O. Tengblad:** Conceptualization, Methodology, Resources, Writing - review & editing, Supervision, Project administration. **I.G. Scheblykin:** Resources, Writing - review & editing. **P. Teubig:** Validation. **R. Timm:** Resources, Writing - review & editing.

Declaration of competing interest

The authors declare that they have no known competing financial interests or personal relationships that could have appeared to influence the work reported in this paper.

Acknowledgments

Discussions with Vladimir Avdeichikov and Bo Jakobsson over several years, preceding this study, are greatly acknowledged as is the work by Oleksandr Bobovnikov to lap the crystal to prepare for the measurements, and the information from Emilie Roncali and Mariele Stockhoff concerning the implementation of LUTs in Geant4 simulations. Tusiime Swaleh is acknowledged for exploring light collection simulations for the project, using a different surface model and crystal geometry than what was finally adopted for the detector and presented in this work. This work was supported by the Swedish research council (VR) grants 2017-03986, 2014-06644, 2013-04178, 2012-04550, BMBF contracts 05P15WOFNA, 05P19WOFN1, 05P15RDFN1, 05P19RDFN1, the TU Darmstadt – GSI cooperation contract HIC for FAIR, by the Spanish research council grants FPA02015-64969-P (MINDECO/FEDER/EU), FPA2015-69640-C2-1-P, PGC2018-099746-B-C21, MDM-2016.0692 (MINECO/FEDER/EU) and by ED431C-2017/54 and EDB481-2017/002 (Xunta de Galicia/FEDER/EU).

References

[1] E. Roncali, S. Cherry, Simulation of light transport in scintillators based on 3D characterization of crystal surfaces, Phys. Med. Bio. 58 (2013) 2185–2198.
[2] M. Stockhoff, et al., Advanced optical simulation of scintillation detectors in GATE V8.0: First implementation of a reflectance model based on measured data, Phys. Med. and Bio. 62 (2017).
[3] J. Bea, et al., Simulation of light collection in scintillators with rough surfaces, Nucl. Instrum. Method Phys. Res. A 350 (1994) 184–191.
[4] A. Knyazev, et al., Properties of the CsI(Tl) detector elements of the CALIFA detector, Nucl. Instrum. and Methods. Phys. Res. A 940 (2019) 393–404.
[5] D. Cortina-Gil, et al., CALIFA, a dedicated calorimeter for the R^3B/FAIR, Nucl. Data Sheets 120 (2014) 99–101, SI.
[6] O. Tengblad, NUSTAR and the status of the R^3B project at FAIR, Pramana 75 (2010) 355–361.
[7] M. Durante, et al., All the fun of the FAIR: fundamental physics at the facility for antiproton and ion research, Phys. Scr. 94 (3) (2019) 033001.
[8] S. Agostinelli, et al., GEANT4 - a simulation toolkit, Nucl. Instrum. Methods Phys. Res. A 506 (3) (2003) 250–303.
[9] J. Allison, et al., GEANT4 developments and applications, IEEE Trans. Nucl. Sci. 53 (1) (2006) 270–278.
[10] J. Allison, et al., Recent developments in Geant4, Nucl. Instrum. Methods Phys. Res. A 835 (2016) 186–225.
[11] M. Janecek, W.W. Moses, Simulating scintillator light collection using measured optical reflectance, IEEE Trans. Nucl. Sci. 57 (3) (2010) 964–970.
[12] M. Janecek, W. W. Moses, Optical reflectance measurements for commonly used reflectors, IEEE Trans. Nucl. Sci. 55 (2008) 2432–2437.
[13] M. Janecek, W. W. Moses, Measuring light reflectance of BGO crystal surfaces, IEEE Trans. Nucl. Sci. 55 (2008) 2443–2449.
[14] H.H. Li, Refractive index of alkaline earth halides and its wavelength and temperature derivatives, J. Phys. Chem. Ref. 9 (1980) 161–290.
[15] P. Schotanus, R. Kamermans, Scintillation characteristics of pure and Tl-doped CsI crystals, IEEE Trans. Nucl. Sci. 37 (2) (1990) 177–182.
[16] Inc. Saint-Gobain Ceramics and Plastics, CsI(Tl), CsI(Na) Cesium Iodide Scintillation material, 2017, Catalogue.
[17] J. Allison, et al., Geant4 electromagnetic physics for high statistic simulation of LHC experiments, J. Phys.: Conf. Ser. 396 (2012) 022013.
[18] V.N. Ivanchenko, et al., Geant4 electromagnetic physics: improving simulation performance and accuracy, in: Proc. SNA + MCA 2013, 2014, 03101.
[19] L. Bergström, Optical properties of deep ice at the South Pole: Scattering, Appl. Opt. 36 (1997) 4181–4194, http://dx.doi.org/10.1364/AO.36.004181.
[20] Hamamtsu Photonics K.K. Solid State Division, Short wavelength type APD, 2017, Catalogue.